Ce-doped NiFe layered double hydroxides coated $NiMoO_xS_{4-x}$ compounds: An efficient OER catalyst in alkaline solution

Nu Wang, Xinyue Wang, Yan Shan, Jia Liu, Jian Zhang, Kezheng Chen, Xuegang Yu**

Lab of Functional and Biomedical Nanomaterials, College of Materials Science and Engineering, Qingdao University of Science and Technology, Qingdao 266042, China.

* Corresponding authors. E-mail addresses: yuxuegang@qust.edu.cn (X. Yu), shanyan@qust.edu.cn (Y. Shan)

Material characterizations

The chemical composition and crystal structure type were confirmed by using an X-ray diffraction (XRD, Rigaku, D/MAX/2500PC) at a scanning rate of 5° min^{-1} ranging from 5° to 80°. The microstructure and morphology of the samples were characterized by using scanning electron microscope (SEM, JEOL JSM-6700F), transmission electron microscope (TEM, JEOL JEM-2100PLUS), and elemental mapping (Energy dispersive X-ray spectroscopy, EDS). The surficial chemical analysis was characterized by X-ray photoelectron spectroscopy (XPS, Thermo ESCALAB XI+). The structural characterization of the electrode was tested through fourier transform infrared spectrometer (FTIR, VERTEX70).

Electrochemical measurements

All tests of electrochemical properties were performed at CHI 660E workstation (CH Instruments, Shanghai), which had a standard three-electrode system in 1M KOH solution. The catalyst, carbon rod and Ag/AgCl electrode were used as working electrode, counter electrode and reference electrode, respectively. The measured potentials were converted to the reversible hydrogen electrode (RHE) on the basis of the Nernst equation: E(RHE) = E (Ag/ AgCl) + 0.2223 + 0.059 × pH. The pH value of the solution is around 14. Before measurement, we measured 200 cycles of cyclic voltammetry (CV) to obtain a stable response, which could make the data more realistic. Then, recorded the linear sweep voltammetry (LSV) date of OER at the scanning rate of 5 mV s^{-1} after iR drop compensation, which the compensation level was 90%. iR compensation is used to compensate for the potential difference caused by the solution resistance. Electrochemical impedance spectroscopy (EIS) was measured at a frequency from 10^{-2} to 10^{5} Hz. Then calculated the over potential (η) of OER exactly by using the equation: η(V) = E(RHE) – 1.23 V and replotted curves as η versus log current density (j) to get Tafel slopes. The estimate of the electrochemically active surface area (ECSA) was conducted by cyclic voltammetry (CV) at a non-Faradaic potential at 20, 40, 60, 80, 100 mV s^{-1} scan rates. ECSA = C_{dl}/ C_s and C_s is a constant of 0.040 mF cm^{-2} in alkaline media. The turnover frequency (TOF) was determined with the equation of TOF = I/(4* F * n) for OER. Here, I is the current density in the LSV scan, 4 corresponds to the two-electron mechanism of the OER process, F is the Faraday constant, n is the moles of Ni atoms assuming that Ni

atoms are active sites.

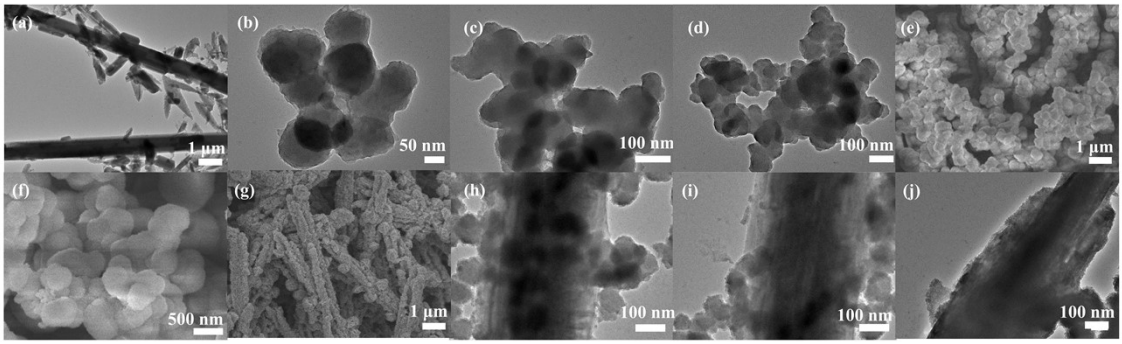

Fig. S1. TEM images of $NiMoO_xS_{4-x}$ (a); Ce-NiFe LDH (b-d); Ce-NiFe LDH@$NiMoO_xS_{4-x}$ (h-j); SEM images of Ce-NiFe LDH (e-f); Ce-NiFe LDH@$NiMoO_xS_{4-x}$ (g).

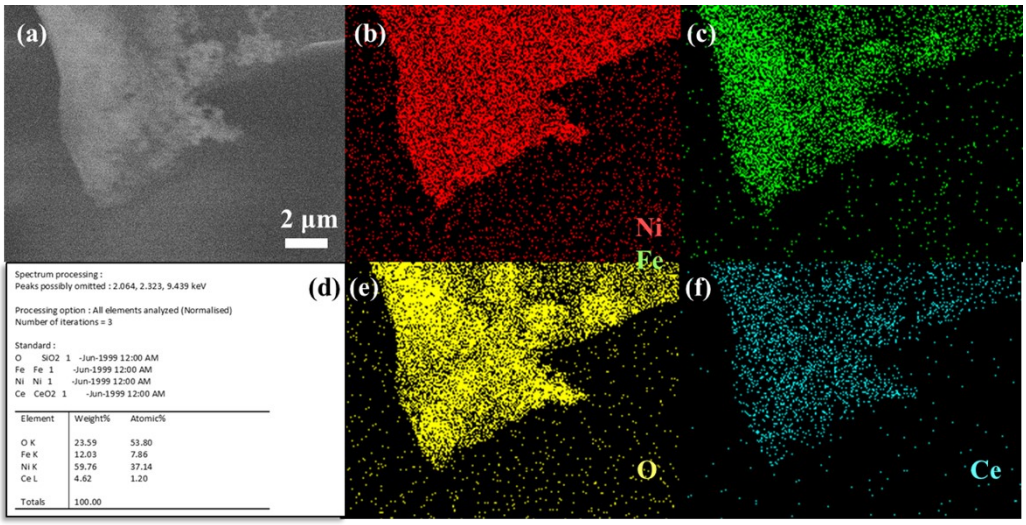

Fig. S2. Elemental mapping images of Ce-NiFe LDH.

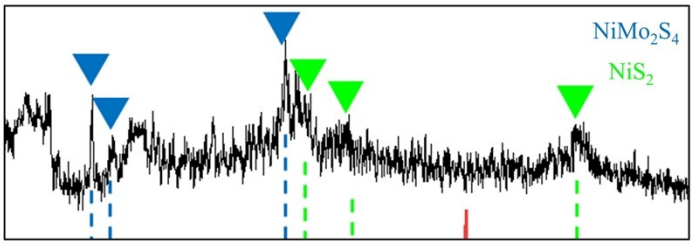

Fig. S3. Amplified pattern of XRD for $NiMoO_xS_{4-x}$.

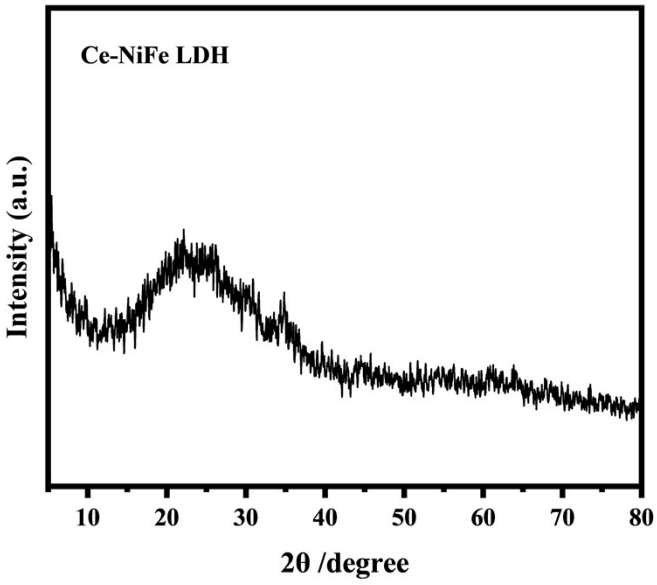

Fig. S4. XRD pattern of Ce-NiFe LDH.

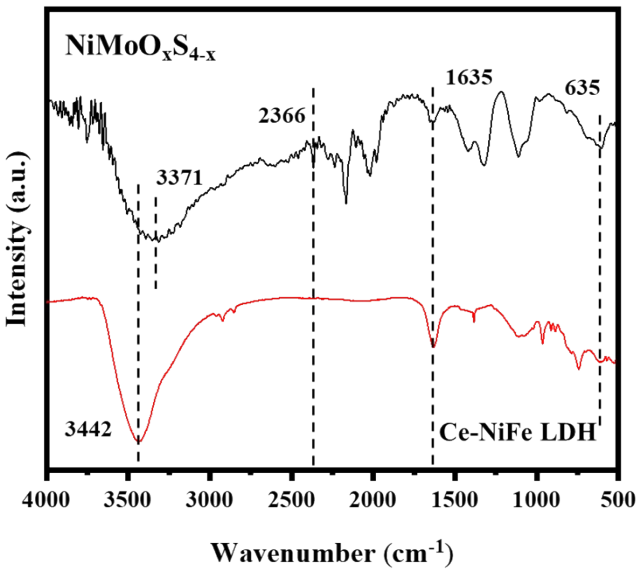

Fig. S5. FT-IR spectra of materials.

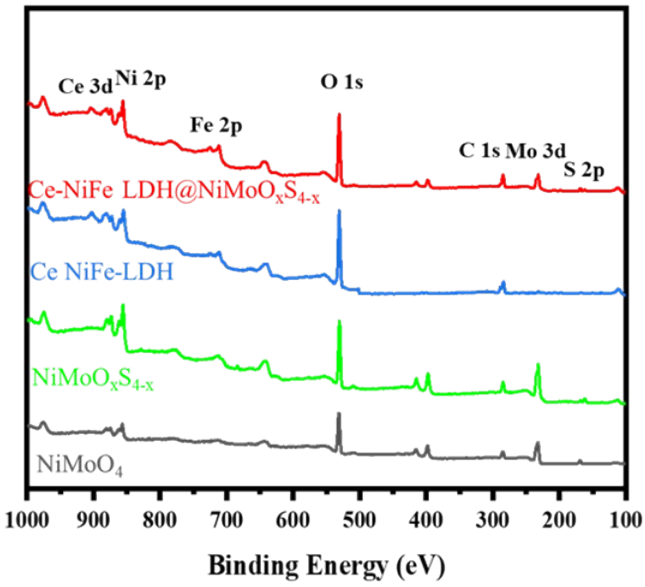

Fig. S6. XPS spectra of various materials.

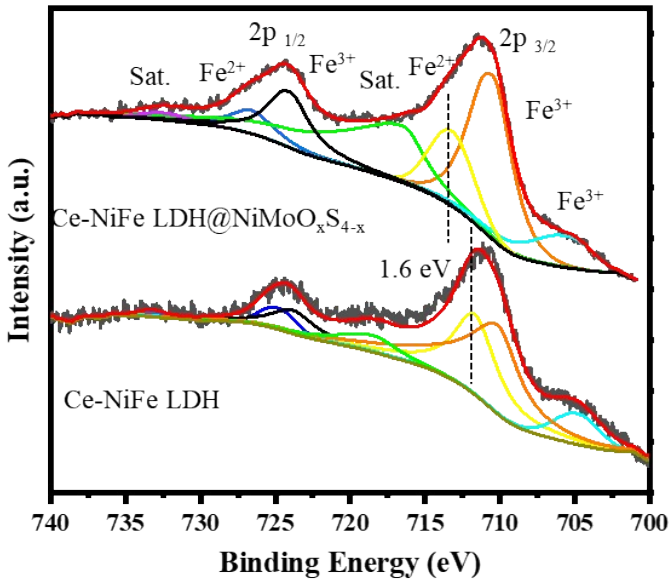

Fig. S7. XPS spectra of Fe 2p in Ce-NiFe LDH@$NiMoO_xS_{4-x}$ and Ce-NiFe LDH.

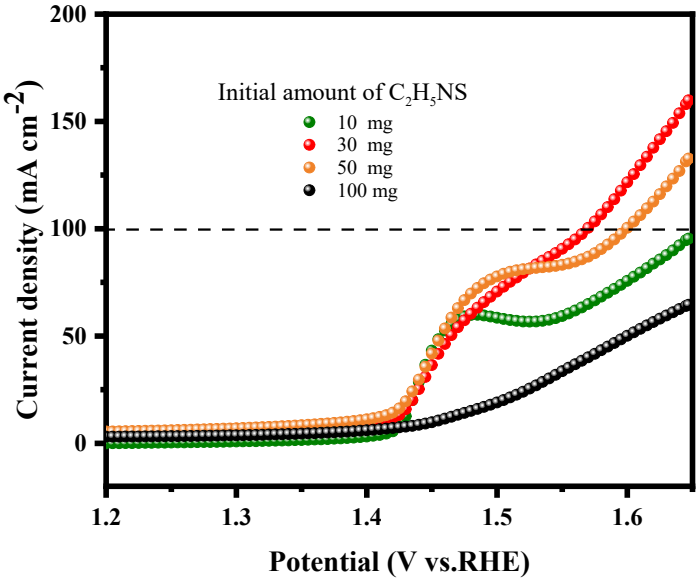

Fig. S8. LSV curves of different initial amount of C_2H_5NS.

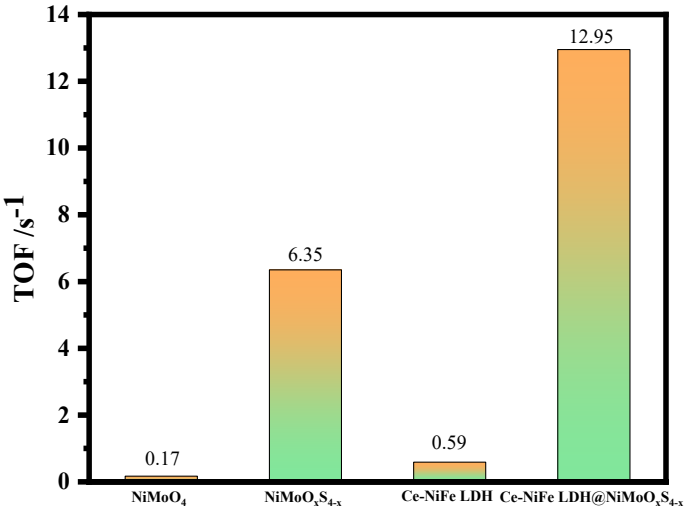

Fig. S9. The TOF values of various catalysts.

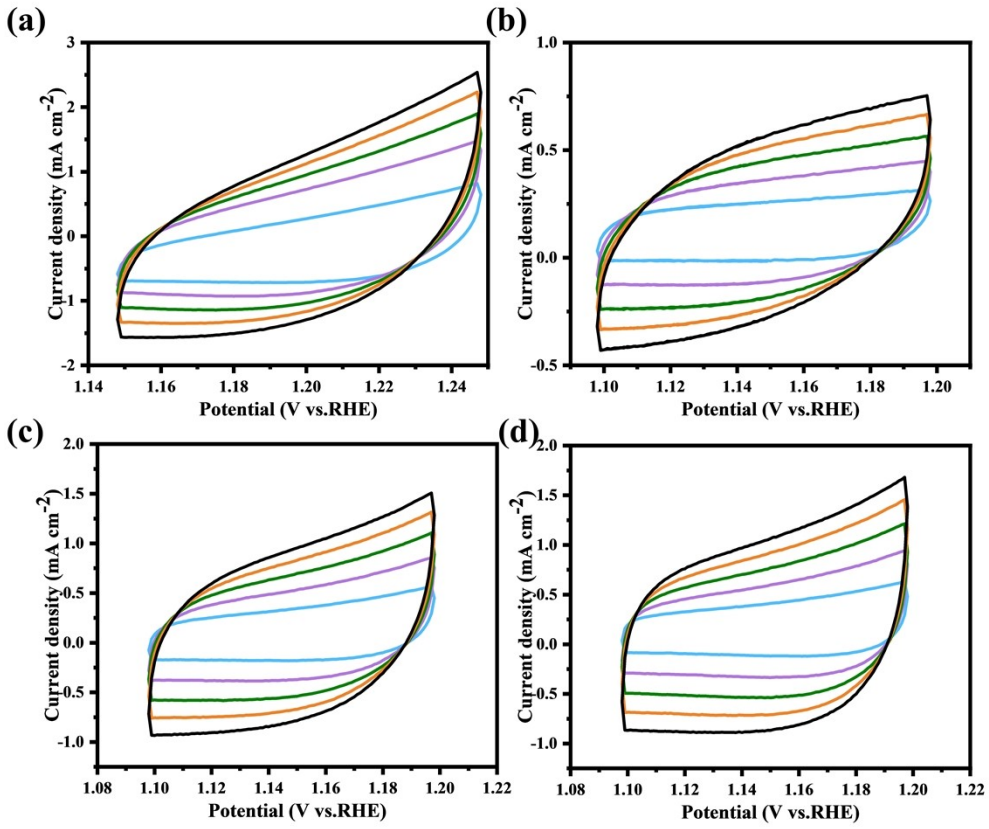

Fig. S10. The CV curves of Ce-NiFe LDH@$NiMoO_xS_{4-x}$ (a), $NiMoO_4$ (b), $NiMoO_xS_{4-x}$ (c), Ce-NiFe LDH (d).

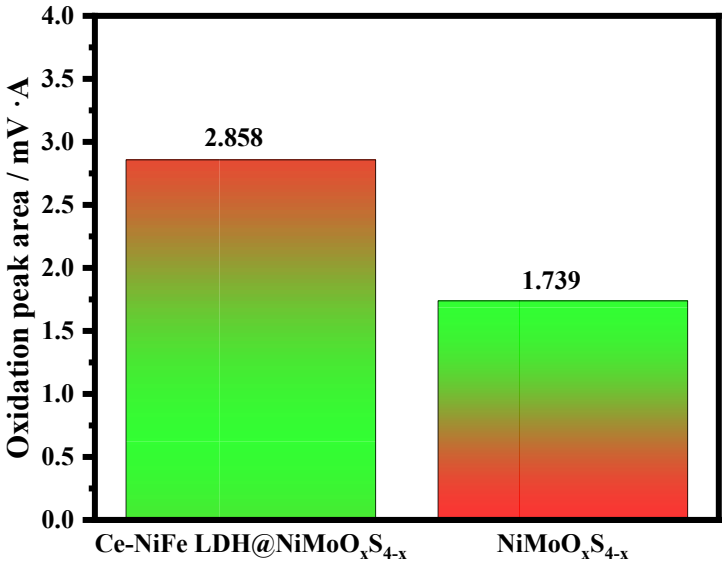

Fig. S11. The oxidation peak areas of Ce-NiFe LDH@NiMoO$_x$S$_{4-x}$ and NiMoO$_x$S$_{4-x}$.

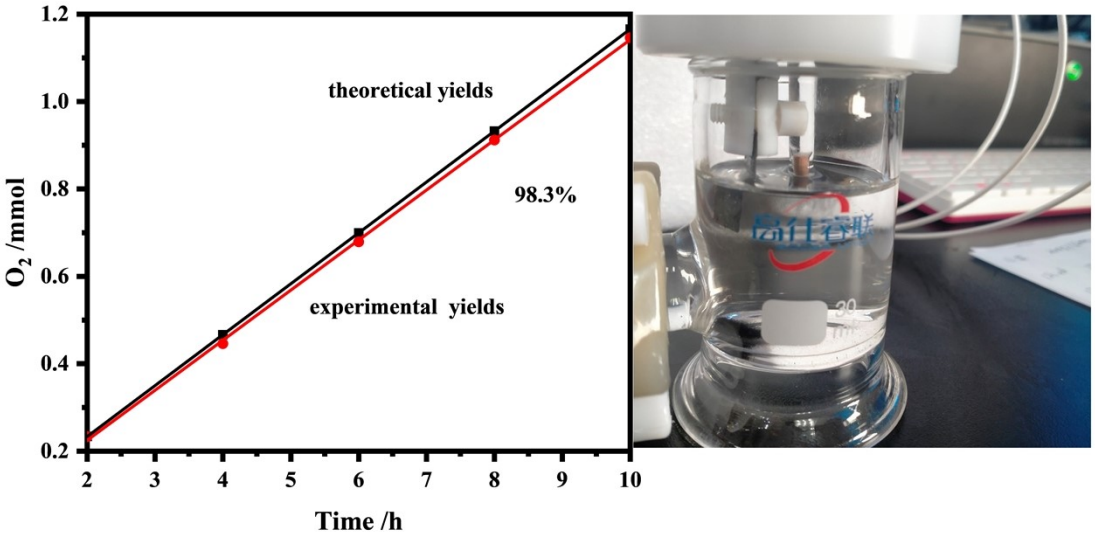

Fig. S12. The OER Faradaic efficiency of Ce-NiFe LDH@NiMoO$_x$S$_{4-x}$.

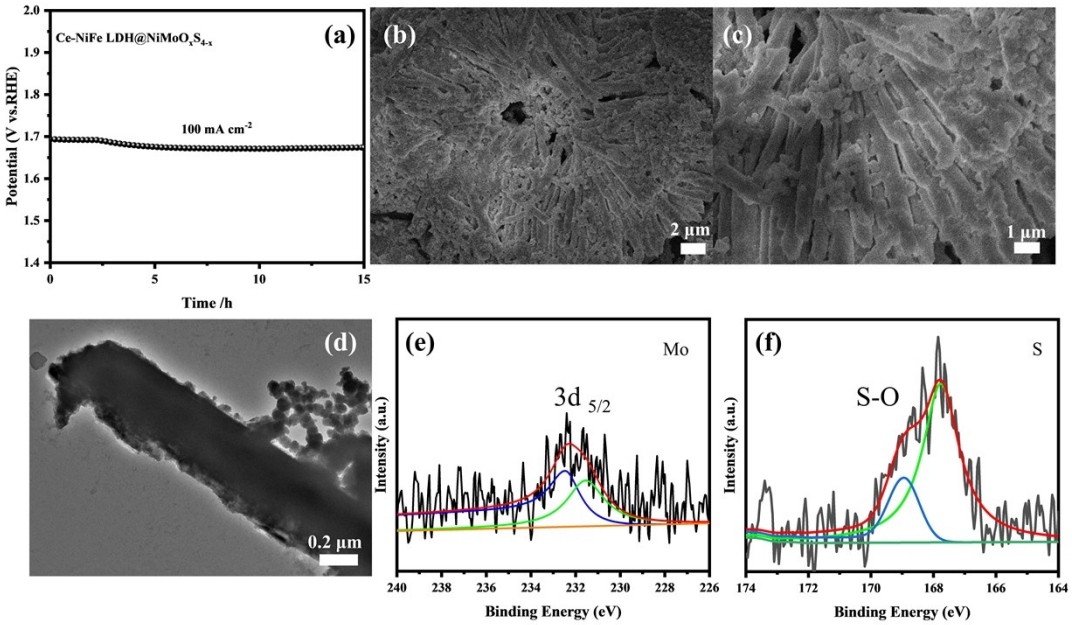

Fig. S13. The chronopotentiometric curve at 100 mA cm^{-2} of Ce-NiFe LDH@$NiMoO_xS_{4-x}$ (a); SEM images (b-d), TEM image (h) and XPS (e-f) of Ce-NiFe LDH@$NiMoO_xS_{4-x}$ after chronopotentiometric test.

Table. S1 OER performance of various electrodes.

Electrode	Overpotential/ mV	Tafel slope /mV dec^{-1}	ECSA/ mF cm^{-2}
$NiMoO_4$	363	51.4	3.52
$NiMoO_xS_{4-x}$	222	92.9	7.47
Ce-NiFe LDH	318	72.1	8.56
Ce-NiFe LDH@ $NiMoO_xS_{4-x}$	190	37.1	9.25

Table. S2 The solution resistances (Rs) and charge transfer resistance (Rct) comparison of.

Electrode	Rs	Rct
$NiMoO_4$	2.0405	4.2130
$NiMoO_xS_{4-x}$	2.0012	2.6958
Ce-NiFe LDH	1.8876	1.9208
Ce-NiFe LDH@ $NiMoO_xS_{4-x}$	1.7474	0.6458

Table 3 Comparison of electrocatalytic activity of recently reported electrocatalysts

Catalysts	Current density (mA cm^{-2})	η(mV)	Ref.
$NiSe_2$/RGO	10	241	[1]
Ni-Fe-Se cages	10	240	[2]
$NiSe_2$/Ni	10	235	[3]
P-$NiSe_2$	10	270	[4]
$NiSe_2$-$Ni_{0.85}Se$/CP	10	300	[5]
NiSe-2	10	252	[6]
Cu-(a-$NiSe_x$/c-$NiSe_2$)/TiO_2 NRs	10	339	[7]
$MoSe_2$-$CoSe_2$@CoAl-LDH	10	320	[8]
Ni_3S_2@NiFe-LDH/NF	10	222	[9]
NiFeCe-LDH/MXene	10	260	[10]
Ce-NiFe LDH@$NiMoO_xS_{4-x}$	100	190	This work

References

[1] Wei P.K, Hao Z.W, Yang Y, *et al*. Unconventional dual-vacancies in nickel diselenide-graphene nanocomposite for high-efficiency oxygen evolution catalysis. Nano. Research. 13 (2020) 3292-3298.

[2] Nai J.W, Lu Y, Yu L, *et al*. Formation of Ni-Fe Mixed Diselenide Nanocages as a Superior Oxygen Evolution Electrocatalyst. Advanced Materials. 29 (2017) 17303870.

[3] Zhang J, Wang Y, Zhang C, *et al*. Self-Supported Porous $NiSe_2$ Nanowrinkles as Efficient Bifunctional Electrocatalysts for Overall Water Splitting. ACS. Sustainable Chem. Eng. 6 (2018) 2231-2239.

[4] Yang W.S, Wang S.S, Zhao K, *et al*. Phosphorus doped nickel selenide for full device water splitting. Journal of Colloid and Interface Science. 602 (2021) 115-122.

[5] Chen Y.J, Ren Z.Y, Fu H.Y, *et al*. NiSe-$Ni_{0.85}Se$ Heterostructure Nanoflake Arrays on Carbon Paper as Efficient Electrocatalysts for Overall Water Splitting. Small. 14 (2018) 1800763.

[6] Feng Z.B, Zhang H, Wang L, *et al*. Nanoporous nickel-selenide as high-active bifunctional electrocatalyst for oxygen evolution and hydrazine oxidation. Journal of Electroanalytical Chemistry. 876 (2020) 114740.

[7] Park K.R, Tran D.T, Nguyen T.T, *et al*. Copper-Incorporated heterostructures of amorphous $NiSe_x$/Crystalline $NiSe_2$ as an efficient electrocatalysts for overall water splitting. Chemical Engineering Journal. 422 (2021) 130048.

[8] Yu C, Cao Z.F, Chen S, *et al*. In situ selenylation of molybdate ion intercalated Co-Al layered double hydrotalcite for high-performance electrocatalytic oxygen evolution reaction. Journal of the Taiwan Institute of Chemical Engineers. 119 (2021) 166-176.

[9] Hu J, Zhu S.L, Liang Y.Q, *et al*. Self-supported Ni_3Se_2@NiFe layered double hydroxide bifunctional electrocatalyst for overall water splitting. Journal of Colloid and Interface Science. 587 (2021) 79-89.

[10] Wen Y.Y, Wei Z.T, Liu J.H, *et al*. Synergistic cerium doping and MXene coupling in layered double hydroxides as efficient electrocatalysts for oxygen evolution. Journal of Energy Chemistry. 52 (2021) 412-420.